

Electronic Supplementary Information: Overcoming the asymmetry of the electron and hole doping for magnetic transitions in bilayer CrI₃

Sukanya Ghosh,^{* a} Nataša Stojić,^a and Nadia Binggeli^a

S1 Planar average plots for electrostatic potential of CrI₃ bilayer without and with 5% uniaxial compressive strain

The planar averages of $V_{\text{local}} + V_{\text{Hartree}}$ along the out-of-plane (z) direction for the unstrained and strained ($\epsilon_{zz} = -5\%$) CrI₃ bilayers in AFM and FM configurations are shown by the black and red curves, respectively, in figure S1. The energy position of the vacuum level is virtually identical for AFM and FM configurations. The difference in vacuum level between AFM and FM configurations is < 0.05 meV. The maximum difference of the electrostatic potential (in the vicinity of the atomic layers) between the AFM and FM configurations is ≈ 1 meV. These are consequences of the total charge density (electronic + ionic) of the AFM and FM bilayers being nearly identical.

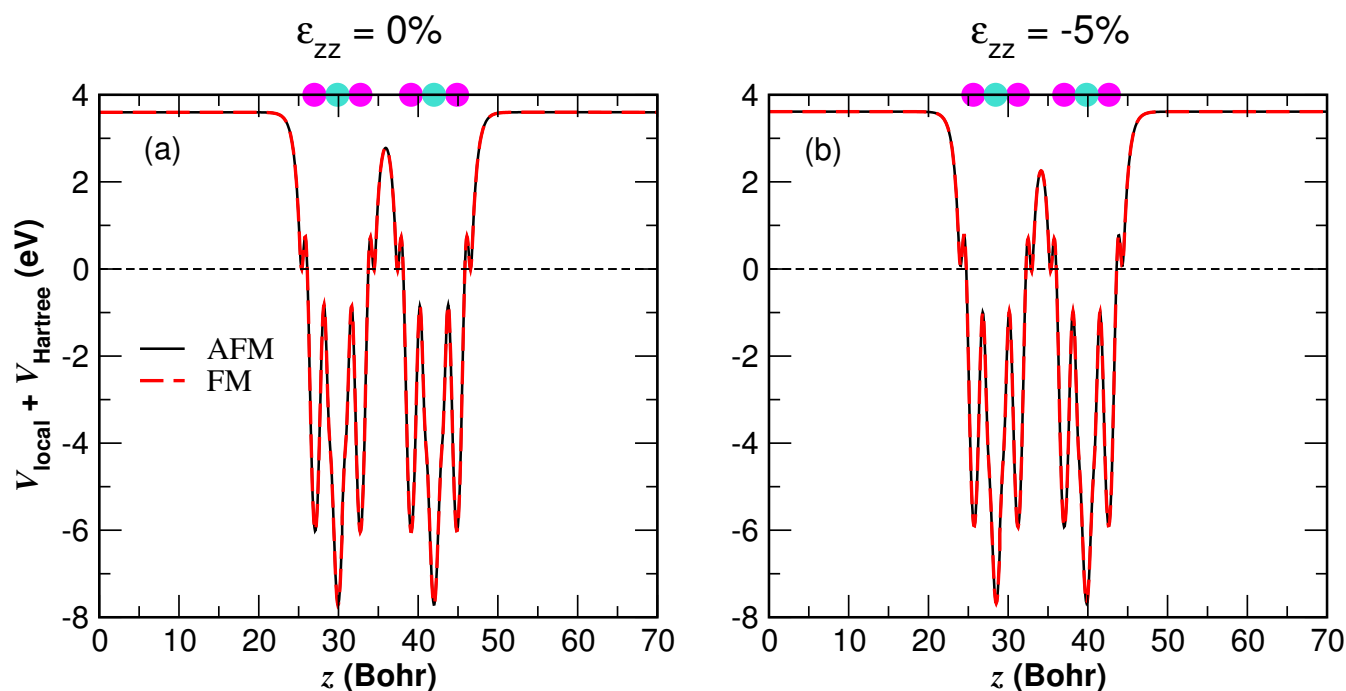


Figure S1: Planar average of the electrostatic ($V_{\text{local}} + V_{\text{Hartree}}$) potential in the supercell for the (a) unstrained ($\epsilon_{zz} = 0\%$) and (b) strained ($\epsilon_{zz} = -5\%$) CrI₃ bilayers in AFM (black curve) and FM (red dashed curve) configurations. The magenta and turquoise spheres show the positions of the iodine and chromium atoms, respectively, along the z direction in the supercell.

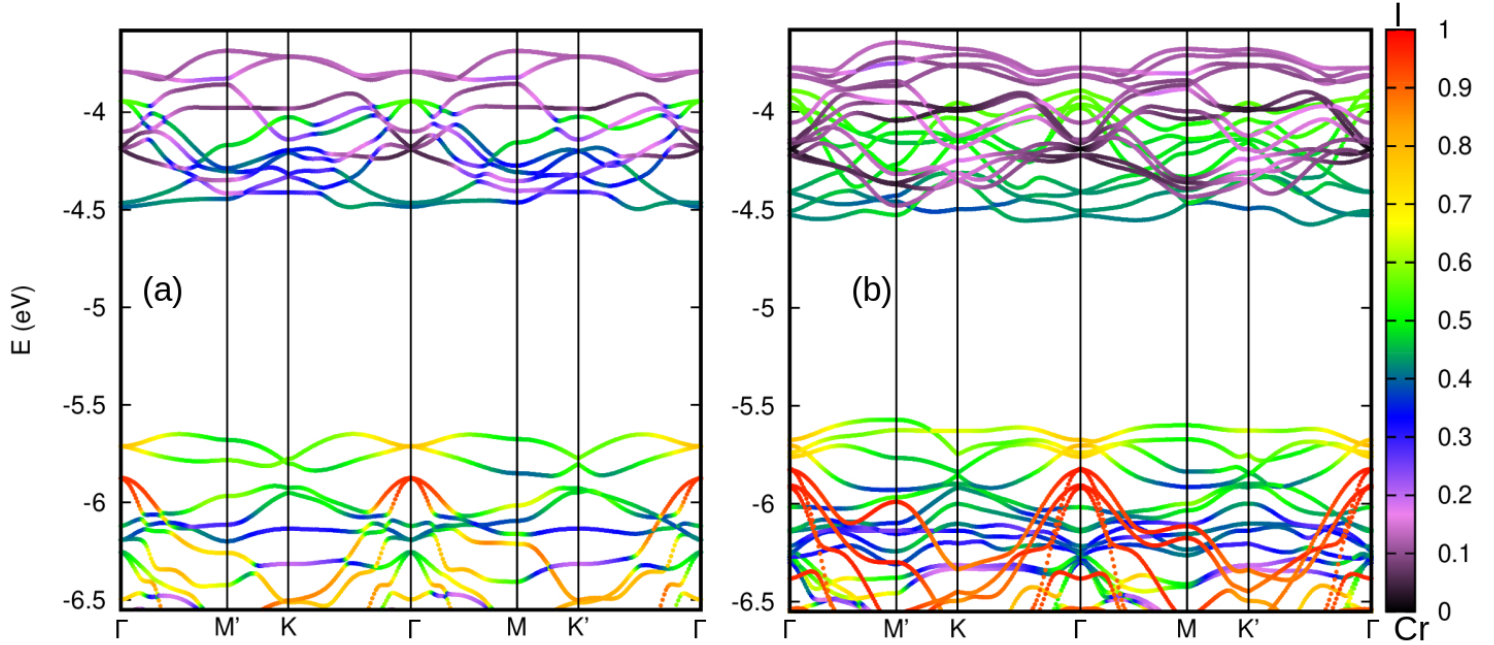


Figure S2: Atomic-projected scalar-relativistic band structure (without spin-orbit coupling) of pristine CrI_3 bilayer in (a) AFM and (b) FM configurations without any strain ($\epsilon_{zz} = 0\%$). The band energies are measured relative to the vacuum potential.

S2 Projected band structures of the pristine CrI_3 bilayer at $\epsilon_{zz} = 0\%$ without spin-orbit coupling

The scalar-relativistic atomic-projected band structures of the CrI_3 bilayer are shown in figure S2 for AFM (a) and FM (b) configurations. As mentioned in the main text of the paper, the group of upper-four valence bands (two 2-fold-degenerate bands in the AFM phase) corresponds predominantly to $\text{Cr-}3d\ t_{2g}$ out-of-plane states with considerable $\text{I-}5p_z$ hybridization, which is further increased in the central part of the BZ. At Γ , the latter atomic-state character is the dominant one for the valence states above -5.8 eV.

S3 Band structures of the doped CrI_3 bilayer at $\epsilon_{zz} = 0\%$ supporting rigid-band model

Relativistic band structure of bilayer CrI_3 in AFM and FM configurations obtained from self-consistent charge-density calculations with 0.1 hole/cell doping is shown in figure S3. The band structure of the doped system and position of the Fermi level in the bands are similar to the results obtained with the rigid-band model of the pristine bilayer, both for the AFM and FM configurations.

S4 Band structure of CrI_3 bilayer with 2% and 4% uniaxial compressive strain

Fully-relativistic band structure plots of CrI_3 bilayer in AFM and FM configurations with 2% and 4% compressive strain (applied along out-of-plane direction) are shown in figures S4(a) – (d). The reduction of the dispersion of the highest valence band in the central part of the BZ and beginning of creation of a new VBM feature around Γ can be observed for increase of the strain from 2 to 4%, in agreement with the trends observed in figures 4 and 5.

^aAbdus Salam International Centre for Theoretical Physics, Strada Costiera, Trieste, Italy; * E-mail: sghosh4@ictp.it

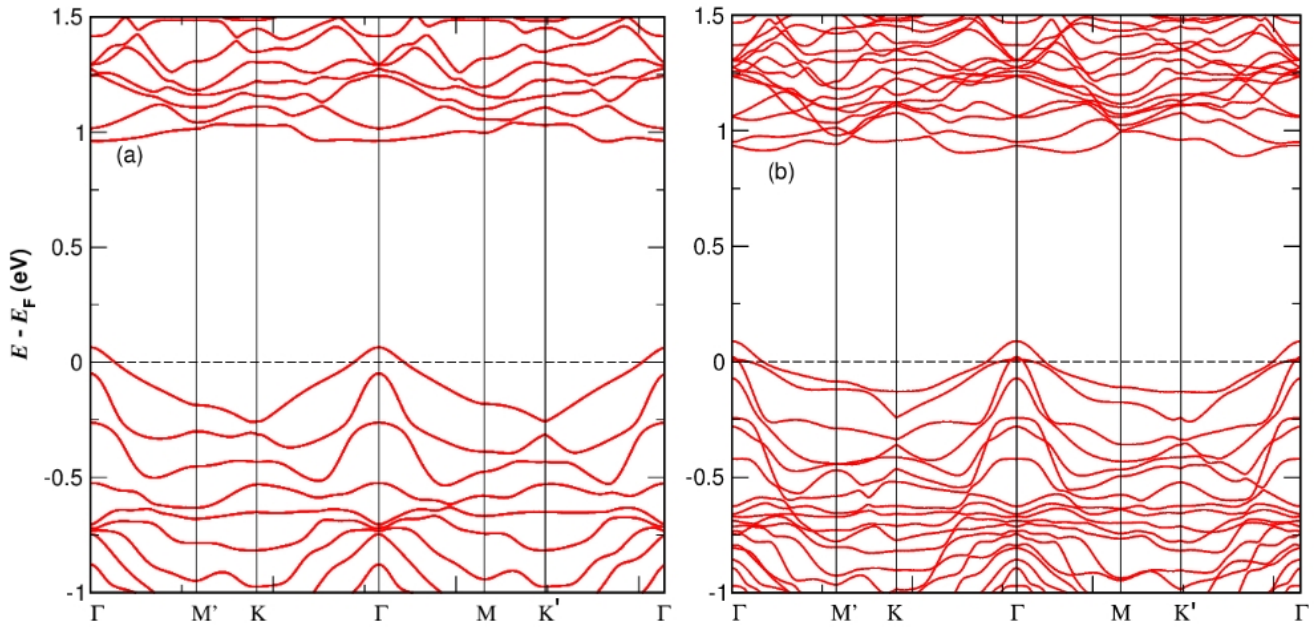


Figure S3: Fully-relativistic band structure plots of the doped CrI₃ bilayer in (a) AFM and (b) FM configurations without any strain ($\epsilon_{zz} = 0\%$) at 0.1 hole/cell doping. The horizontal dashed line corresponds to the Fermi energy.

S5 Band structure of CrI₃ bilayer with disentangled effects of d_{int} and d_{intra} contractions

Relativistic band structure plots of the bilayer obtained by reducing separately the interlayer and intralayer distances d_{int} and d_{intra} are shown in figure S5 in FM configuration. The values of d_{int} and d_{intra} for the unstrained bilayer are 3.36 Å and 3.06 Å, respectively. Under the application of 5% out-of-plane compressive strain d_{int} and d_{intra} reduce to 3.07 Å and 2.96 Å, respectively. To find out which of these two parameter changes plays the dominating role in modifying the electronic structure of the bilayer under the application of the vertical strain, we have disentangled their effects on the electronic band structure of the bilayer.

The band structure plots for (a) $d_{\text{int}} = 3.07$ Å, $d_{\text{intra}} = 3.06$ Å and (b) $d_{\text{int}} = 3.36$ Å, $d_{\text{intra}} = 2.96$ Å are shown in figure S5. From figure S5, one can see that the band structure for strained d_{int} and unstrained d_{intra} , displayed in figure S5(a), is much more similar overall to the band structure of the bilayer with -5% strain (figure 5(b) in the manuscript) than the band structure of the strained d_{intra} and unstrained d_{int} , shown in figure S5(b) [which, in turn, is much more similar to the band structure of the unstrained bilayer (figure 4(b) of the manuscript)]. Comparison of these band structures shows that the band-structure changes induced by the 5% compression of the bilayer are dominated by the effect of the d_{int} contraction. In particular, inspection of the upper part of the valence band structures shows that the occurrence of the pronounced new local valence band maxima around Γ in the 5%-strained bilayer (see figure 5), which enables the AFM-FM transition upon hole doping, is due to the reduction of d_{int} .

S6 Electronic density of states for CrI₃ bilayer with 0% and 5% uniaxial compressive strain

Figure S6 shows the fully-relativistic electronic density of states (DOS) for the unstrained and strained (5% compressive strain) CrI₃ bilayer in AFM and FM configurations. In comparison to DOS of the pristine bilayer in figure S6 (a) and (b), a large increase of DOS at the VBM can be seen upon the compression, see figures S6(c) and (d), especially in the FM case. Furthermore, it can be observed that the broadening of the FM valence and conduction bands is larger than for the AFM configuration, supported by the positions of Fermi level for 0.1 e(h) doping. Similar conclusion was reached for the band structures shown in figure 5. The uniaxial compressive

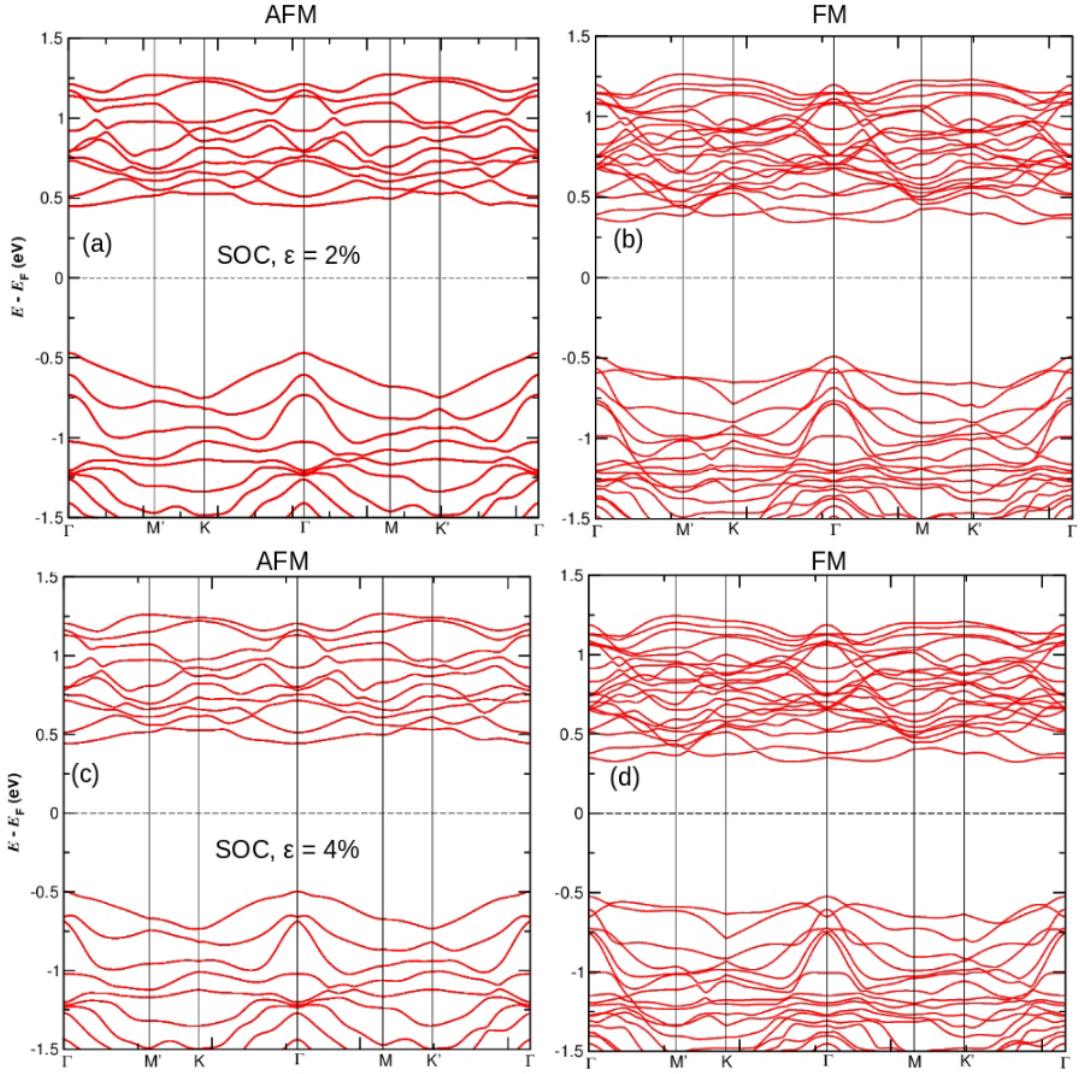


Figure S4: Fully-relativistic band structure of CrI₃ bilayer under (a), (b) 2% and (c), (d) 4% uniaxial compressive strain in AFM and FM configurations.

strain causes the $J_z = |0.5|$ states to shift towards higher energy in the valence band, i.e., moves close to the Fermi energy, as indicated by the arrows in figure S6.

S7 Validation of rigid-band model for doped CrI₃ bilayer at $\epsilon_{zz} = -5\%$

Fully-relativistic band structure of bilayer CrI₃ in AFM and FM configurations under 5% compressive strain from self-consistent charge-density calculations with 0.1 hole/cell doping is shown in figures S7 (a) and (b). The corresponding band structure in FM configuration for 0.1 electron/cell doping at $\epsilon_{zz} = -5\%$ is shown in figure S7(c). The band structures of the doped systems and positioning of the Fermi level in the bands are similar to the results obtained with the undoped bilayer and rigid-band model, both for the AFM and FM configurations.

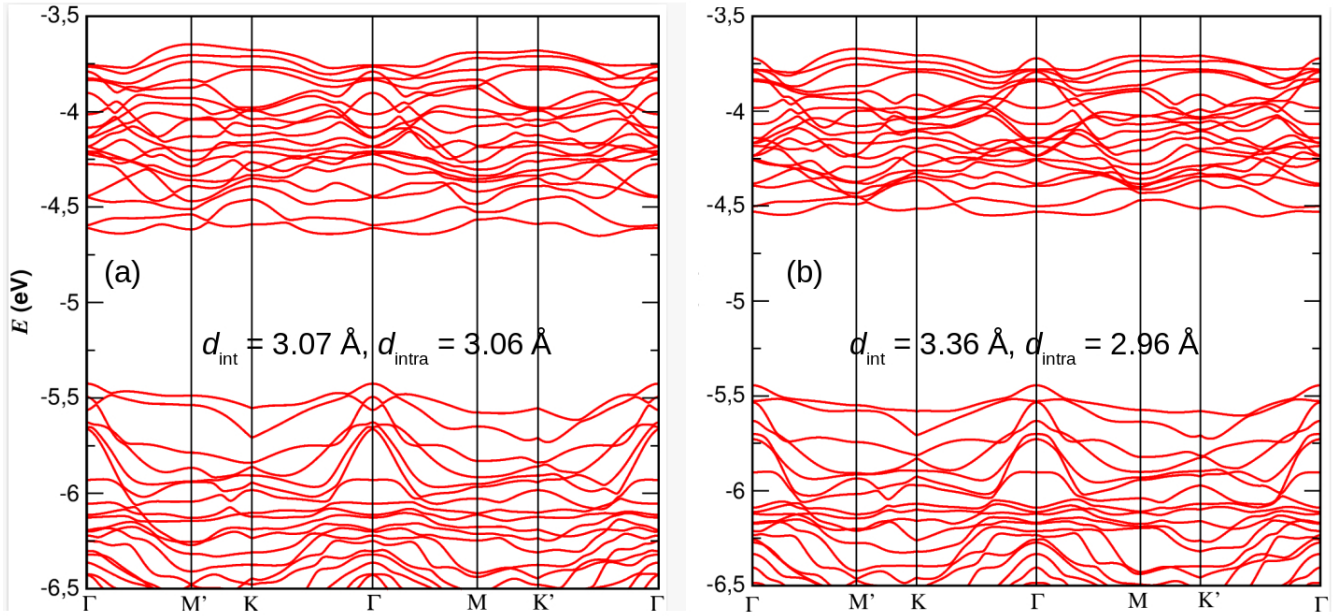


Figure S5: Fully-relativistic band structure plots of the undoped CrI₃ bilayer for (a) $d_{\text{int}} = 3.07 \text{ \AA}$, $d_{\text{intra}} = 3.06 \text{ \AA}$ and (b) $d_{\text{int}} = 3.36 \text{ \AA}$, $d_{\text{intra}} = 2.96 \text{ \AA}$ in FM configuration.

S8 Comparison between band-offset model predictions and computed values of E_{ex} changes with doping in CrI₃ bilayer

Table 1: Comparison between $\Delta E_{\text{ex}}^{\text{model}}$ and $\Delta E_{\text{ex}}^{\text{DFT}}$ for different values of ε_{zz} in the presence and absence of spin-orbit-coupling (SOC). $\Delta \varepsilon_F = \varepsilon_{\text{AFM}} - \varepsilon_{\text{FM}}$ is the difference in Fermi energy between AFM and FM configurations at the conduction (valence) band edge for electron (hole) doping. $E_{\text{ex}} = E_{\text{FM}} - E_{\text{AFM}}$ is the exchange energy of the bilayer. $\Delta E_{\text{ex}}^{\text{model}}$ is obtained using: $\Delta \varepsilon_F \times \text{doping}$. $\Delta E_{\text{ex}}^{\text{DFT}} = E_{\text{ex}}^{\text{doped}} - E_{\text{ex}}^{\text{undoped}}$ is the difference in exchange energies between the doped and undoped CrI₃ bilayer from DFT calculations.

Exc-functional	ε_{zz}	Doping concentration (/cell)	$\Delta \varepsilon_F$ (meV per electron)	$\Delta E_{\text{ex}}^{\text{model}} = \Delta \varepsilon_F \times \text{doping}$ (meV/cell)	$\Delta E_{\text{ex}}^{\text{DFT}}$ (meV/cell)
LDA+SOC	0%	0.1 h	2.6	-0.26	-0.24
		0.1 e	55.1	5.51	6.32
	-5%	0.1 h	-24.0	2.40	2.82
		0.1 e	60.0	6.00	7.444
LDA	0%	0.1 h	-56.10	5.61	6.15
		0.1 e	70.7	7.07	6.73

In Table 1, we compare our model predictions for the change in the exchange-coupling energy with doping, $\Delta E_{\text{ex}}^{\text{model}}$, based on the band-edge-offset $\Delta \varepsilon_F$ values (i.e., the difference between the ε_F of the AFM and FM bilayer, each measured relative to the vacuum potential) with the computed values $E_{\text{ex}}^{\text{DFT}}$ of the doping-induced changes in E_{ex} . The model describes the changes in E_{ex} upon doping, $\Delta E_{\text{ex}} = E_{\text{ex}}(\text{doped}) - E_{\text{ex}}(\text{undoped})$, as $\Delta E_{\text{ex}}^{\text{model}} = \Delta \varepsilon_F \times \text{doping}$. The computed values $E_{\text{ex}}^{\text{DFT}}$ and the model predictions $\Delta E_{\text{ex}}^{\text{model}}$ are reported in the table for 0.1 hole/cell and 0.1 electron/cell doping, both for the unstrained and strained bilayer with SOC and also for the unstrained bilayer without SOC.

It is evident from Table 1 that in all cases our proposed model, $\Delta E_{\text{ex}}^{\text{model}} = \Delta \varepsilon_F \times \text{doping}$, not only qualitatively describes the trends of the exchange-coupling energy with doping, but actually also predicts quite well (within 20%) the values of the changes in E_{ex} upon electron (hole) doping. Moreover, as we stated in the main text of the paper, the values of ε_F are nearly identical for 0.1 and 0.2 hole (electron)/cell doping, compared

to the much larger energy value of the dominant (conduction) band-offset offset ($\Delta\epsilon_F^c$) between the AFM and FM bilayers. Hence, $\Delta\epsilon_F$ is essentially a constant [with a small first-order correction term $O(\text{doping})$, which in the model, $\Delta E_{\text{ex}} = \Delta\epsilon_F \times \text{doping}$, yields for ΔE_{ex} a negligible second-order correction term $O(\text{doping}^2)$] for doping up to 0.2 hole (electron) /cell. The model thus also explains the linear dependence of E_{ex} with electron (hole) doping which we observe in the *ab initio* calculations.

S9 3D isosurface and planar average plots for the probability density of the upper valence states in the pristine and strained bilayer

Figure S8 shows the 3D isosurface plots for the probability density, $|\Psi|^2$, of the upper three valence bands in AFM pristine configuration (a)–(c) and with 5% compression (d)–(f). In the case of the unstrained bilayer $|\Psi|^2$ for the upper three valence bands are plotted at Γ , corresponding to the VBM position. Since the local VBM for the 5% compression is along $\Gamma - M$ direction, outside Γ , we plotted $|\Psi|^2$ for the upper valence bands at the position of the new local VBM. The highest 2 bands (figure S8 (a-b)) in the pristine bilayer display predominant in-plane character of the states located on the I atoms, while the probability density for the third band (figure S8 (c)) shows much more out-of-plane features. Upon addition of the compressive perpendicular strain, the local VBM is characterized by states with more pronounced out-of-plane character on the atoms of the inner I planes of the bilayer (figure S8 (a-b)).

Figure S9 shows the planar average plots for $|\Psi|^2$ of the upper three valence bands in the pristine and strained AFM configuration. It can be observed that in the pristine bilayer the highest lying two bands have the states localized on one of the layers of the bilayer, on the I atoms. The third band, on the other hand shows a stronger probability density in the Cr region and much more extended probability density in the space between the layers. The states of the highest two bands in the strained bilayer, outside Γ , bear significant resemblance to the states of the third-upper band at Γ in the unstrained bilayer.

In figure S10 we show the 3D isosurface plots for the probability density of the upper three valence bands in the pristine (at Γ) and strained FM configuration (near Γ , in the $\Gamma M'$ direction). The corresponding planar average plots of the probability densities are shown in figure S11. Similar to the AFM case, in the pristine bilayer the highest four states have dominant I in-plane character (figures S10 and S11), while the next two valence states have strong out-of-plane probability density, in particular on the I atoms of the inner I planes of the bilayer. For the strained bilayer, the highest four states outside Γ have pronounced out-of-plane features. These states, and particularly the upper two states, resemble the fifth and sixth upper valence states at Γ of the unstrained FM bilayer.

Hence, both for the FM and AFM bilayers, the pristine systems show a VBM characterized by in-plane I states, while the application of the compressive strain induces a new local VBM for which the states display significant out-of-plane orbitals on the atoms of the I inner planes of the bilayer.

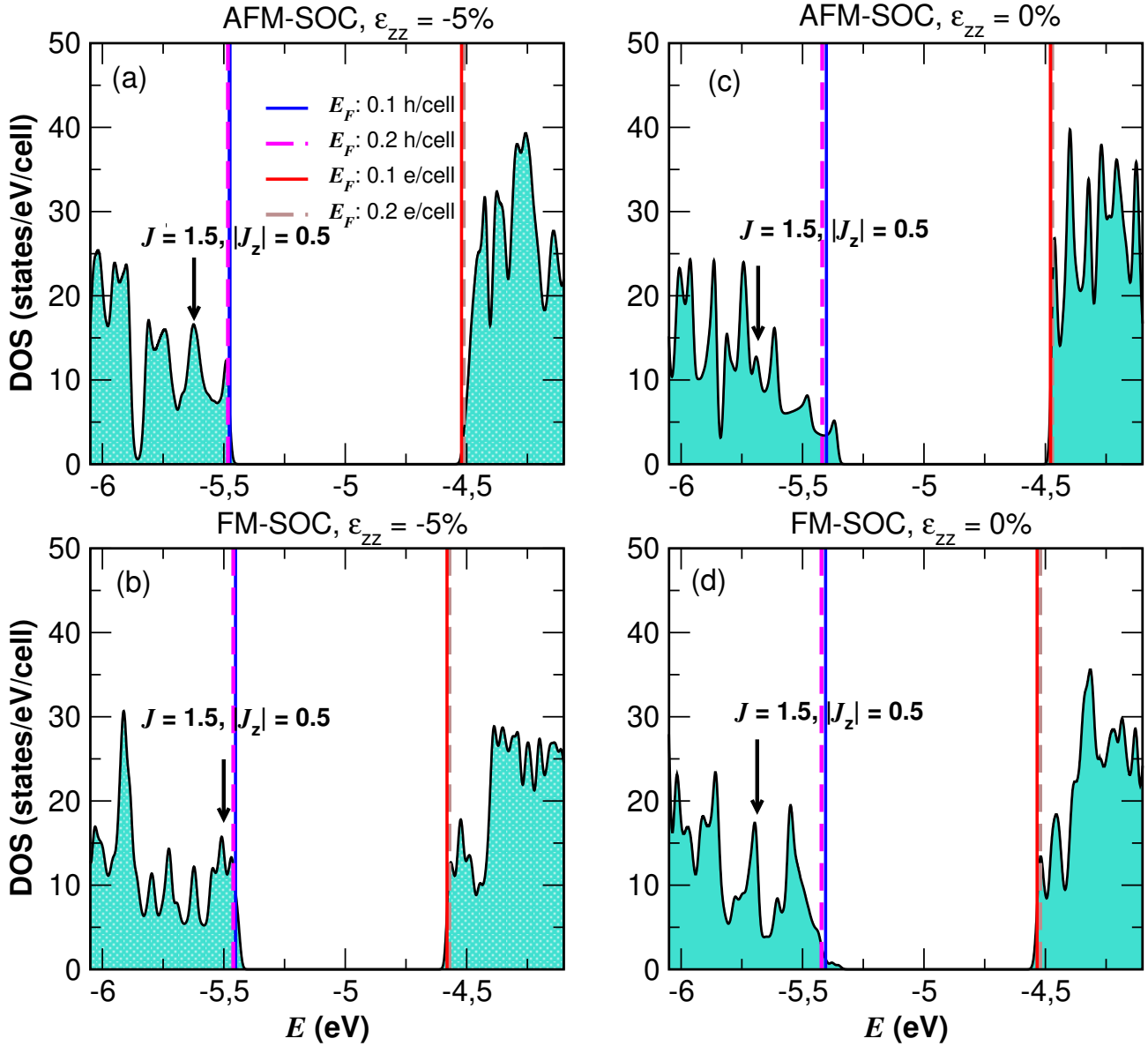


Figure S6: Electronic density of states of bilayer CrI_3 (including SOC) under (a)–(b) 0% and (c)–(d) 5% compressive uniaxial strain for (a), (c) AFM and (b), (d) FM configurations. The energy is given with respect to the vacuum potential. The vertical solid blue, dashed magenta, solid red and dashed brown lines are the Fermi energies corresponding to 0.1 hole/cell, 0.2 hole/cell, 0.1 e/cell and 0.2 e/cell doping, respectively, obtained from rigid-band model. The vertical black arrow in each plot shows the energy level with $J = 1.5, |J_z| = 0.5$ (pointing by the black arrow). The uniaxial compressive strain causes the $|J_z| = 0.5$ states in the valence band to rise up in energy.

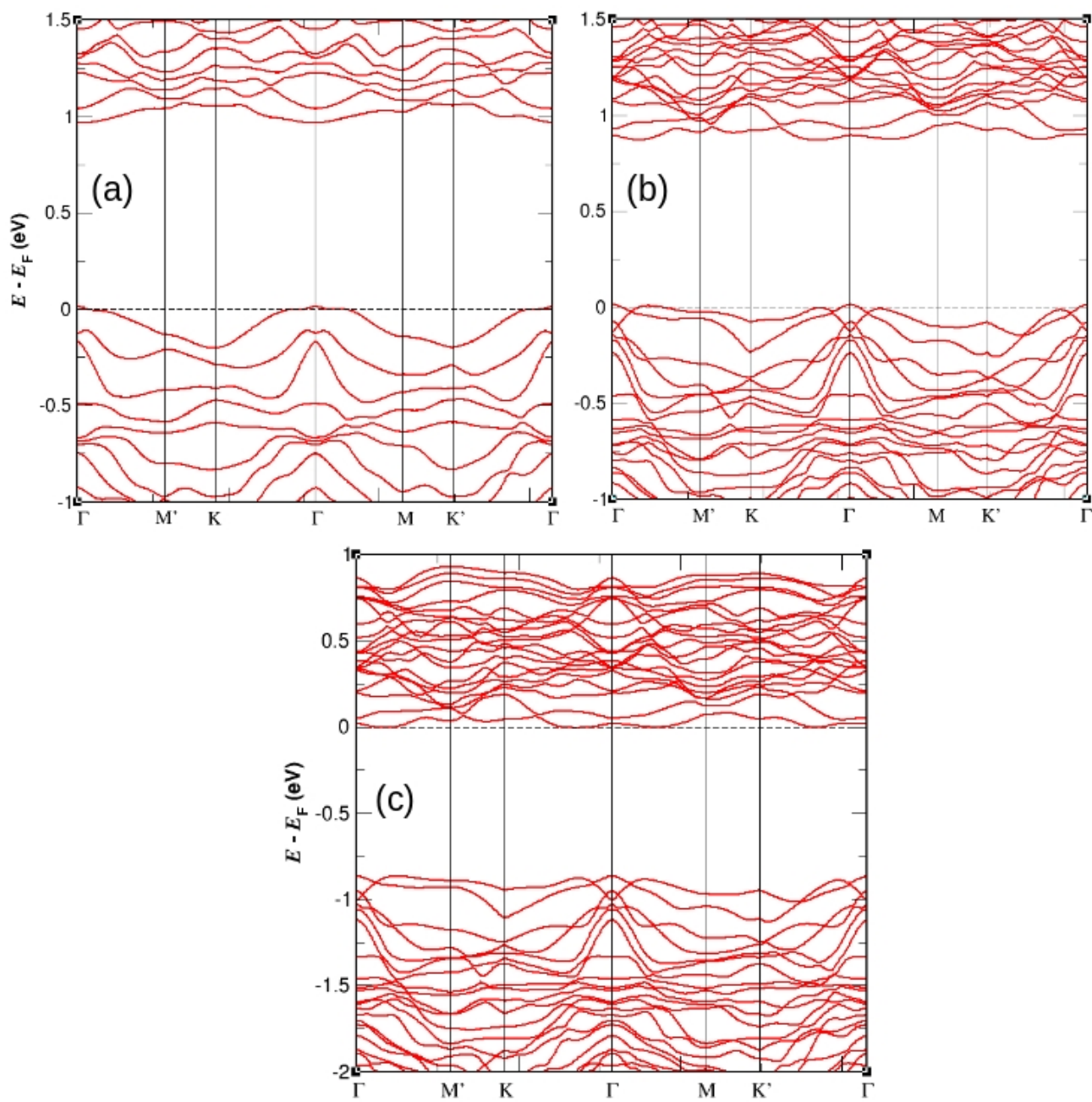


Figure S7: Fully-relativistic band structure of doped CrI₃ bilayer under 5% compressive strain: (a) AFM and (b) FM configurations with 0.1 hole/cell doping, and (c) FM configuration at 0.1 electron/cell doping. The horizontal dashed line in each plot corresponds to the Fermi energy.

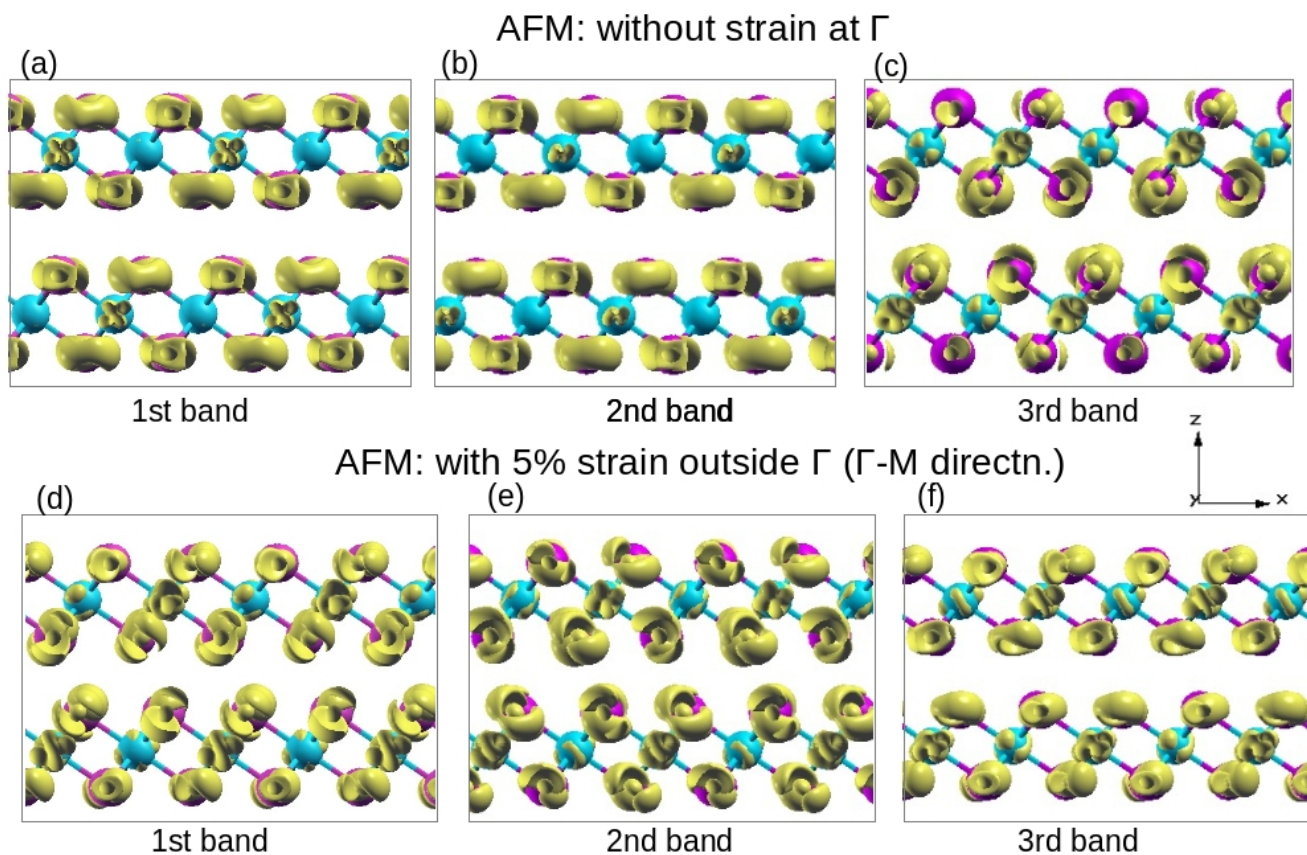


Figure S8: 3D iso-surface plots of the probability density for the upper valence states of CrI_3 bilayer in AFM configuration. (a)–(c) Unstrained bilayer at Γ and (d)–(f) strained (5%) bilayer outside Γ along $\Gamma - M$ direction. (a) and (d): first upper valence band; (b) and (e): second upper valence band; (c) and (f): third upper valence band for the unstrained and strained CrI_3 bilayers, respectively. Drawn at iso-surface value = $0.002 e/\text{Bohr}^3$.

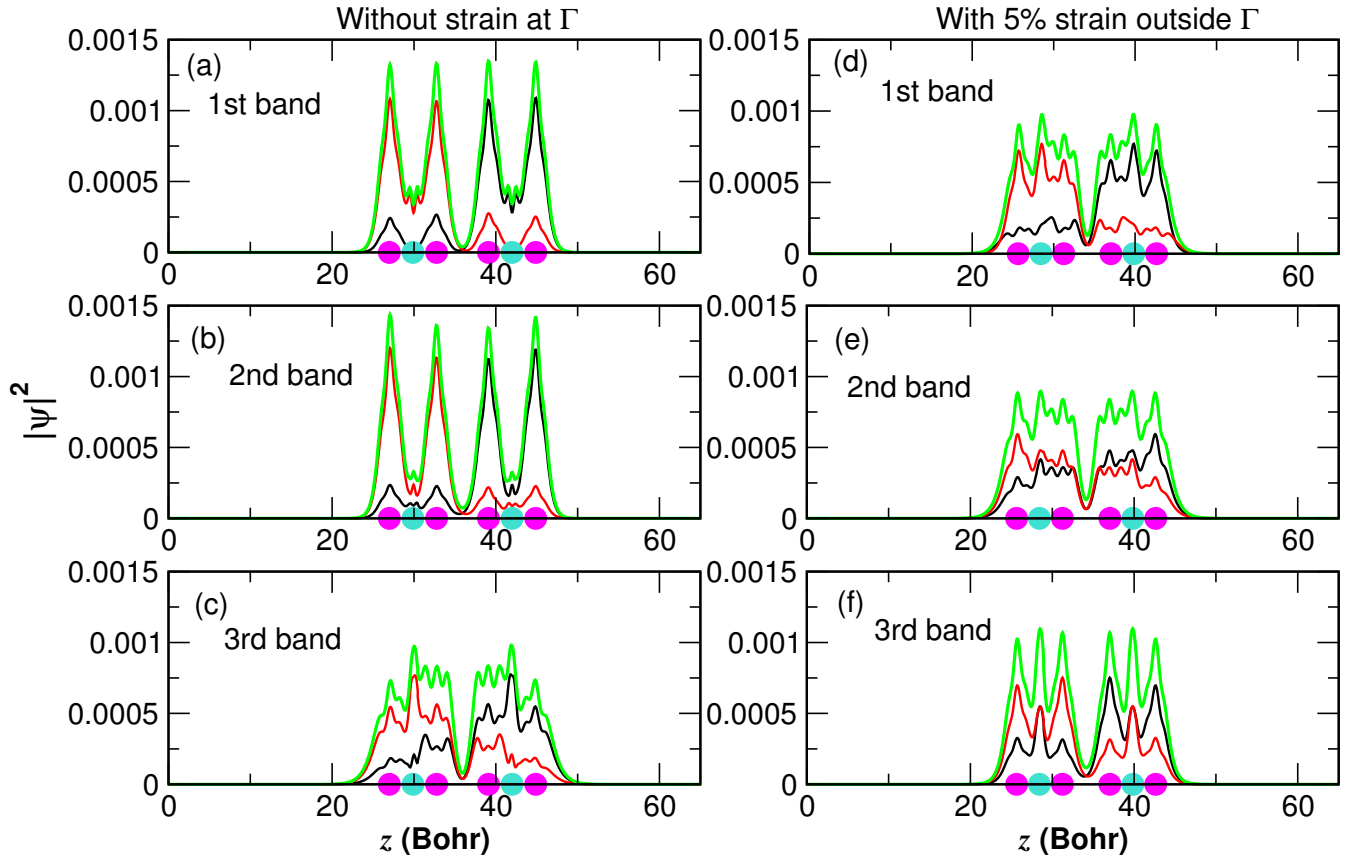


Figure S9: Planar average plots of the probability density for the first three upper valence bands of the pristine and strained AFM CrI_3 bilayer. (a)–(c) Unstrained bilayer at Γ and (d)–(f) compressed (5%) bilayer outside Γ (along $\Gamma - M$ direction). (a) and (d) First upper valence band; (b) and (e) second upper valence band; (c) and (f) third upper valence band for the unstrained and strained systems, respectively. The black and red curves correspond to the degenerate states belonging to a particular band, the green curve is the sum.

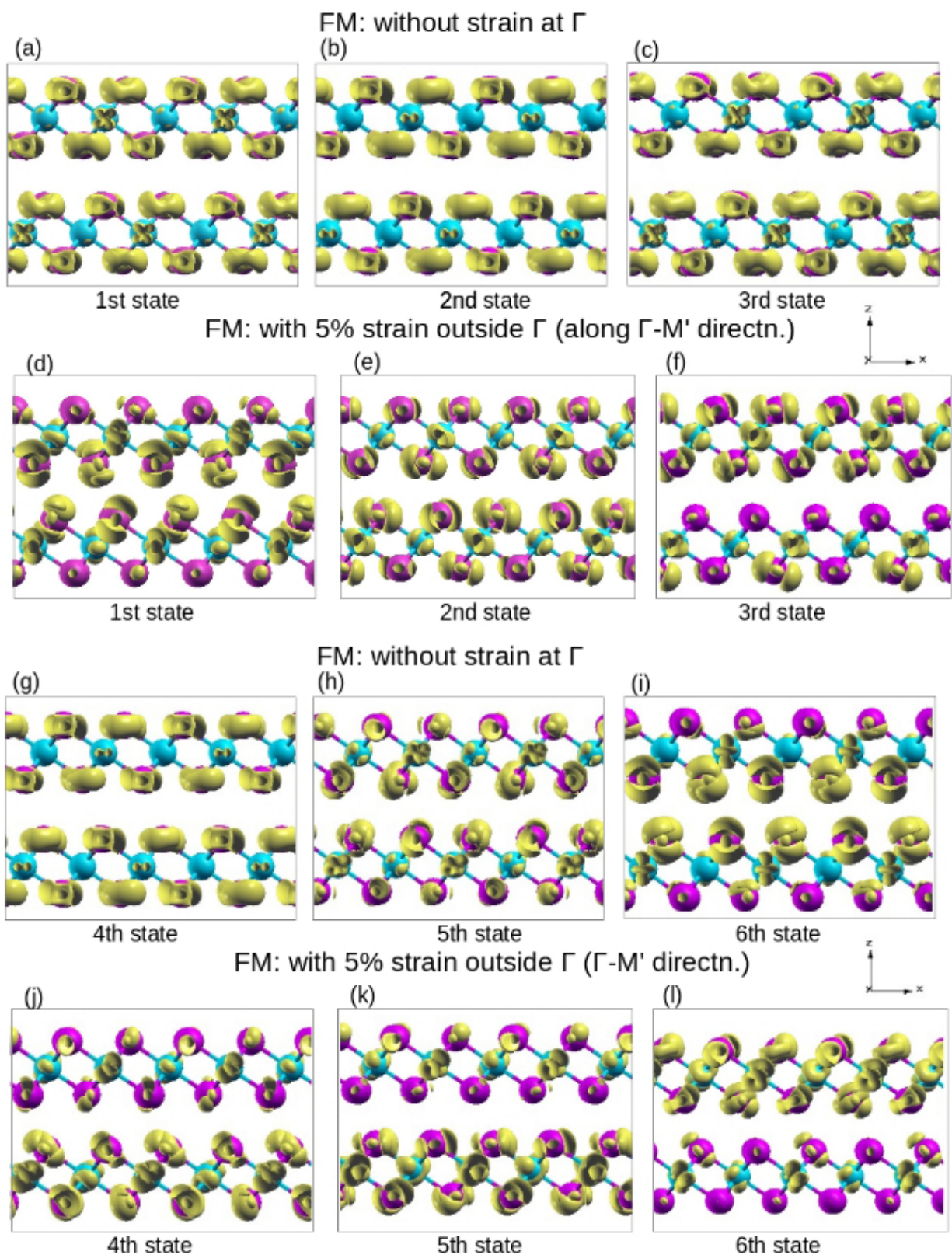


Figure S10: 3D iso-surface plots of the probability density for the upper valence states of CrI_3 bilayer in FM configuration. (a)–(c) and (g)–(i) Unstrained bilayer at Γ , (d)–(f) and (j)–(l) strained (5%) bilayer outside Γ along $\Gamma - M'$ direction. (a) and (d): first upper valence state; (b) and (e): second upper valence state; (c) and (f): third upper valence state; (g) and (j): fourth upper valence state; (h) and (k): fifth upper valence state; (i) and (l): sixth upper valence state for the unstrained and strained CrI_3 bilayers, respectively. Drawn at iso-surface value = $0.001 e/\text{Bohr}^3$.

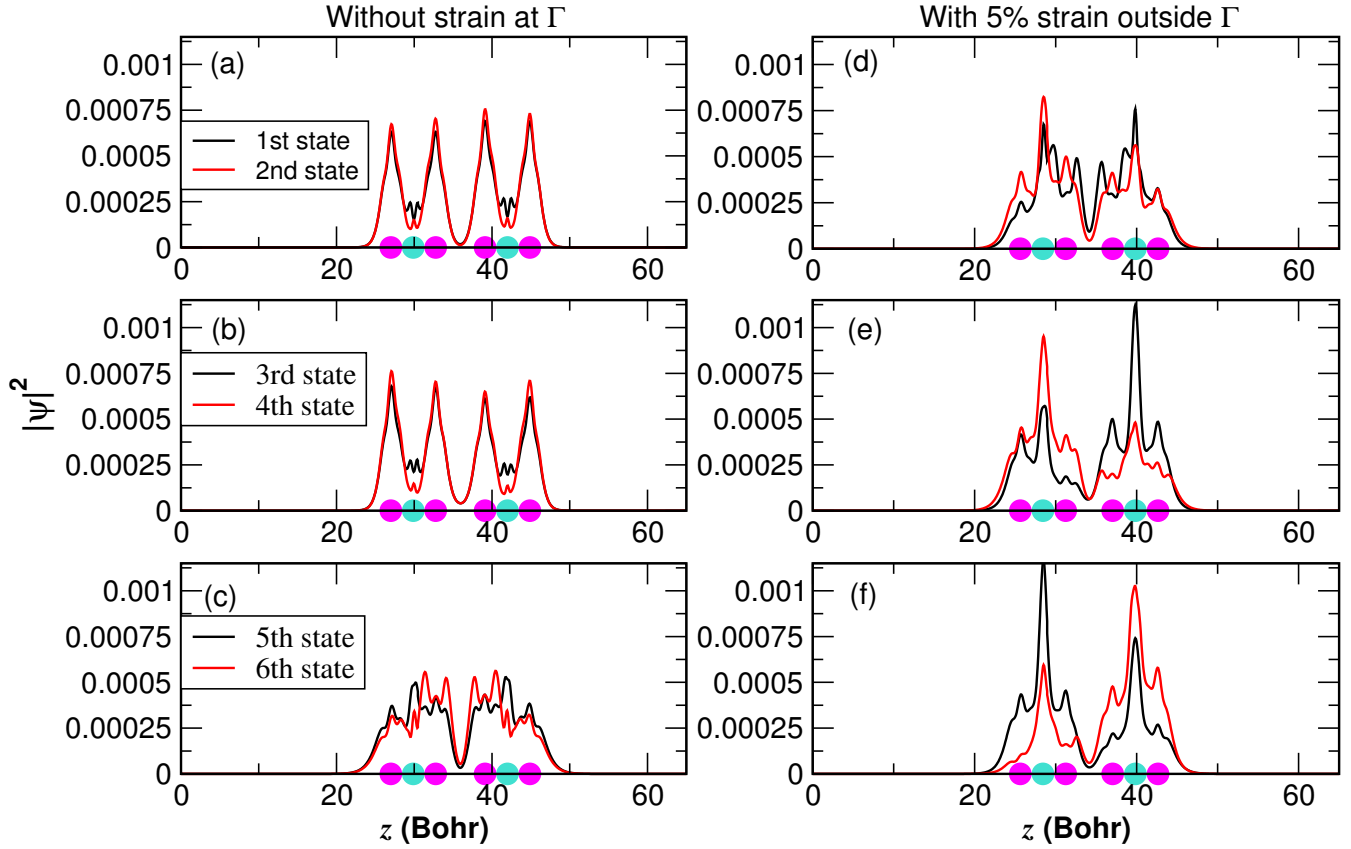


Figure S11: Planar average plots of the probability density for the upper six valence bands of the pristine and strained CrI_3 bilayer in FM configuration. (a)–(c) Unstrained bilayer at Γ and (d)–(f) strained bilayer outside Γ (along $\Gamma - M'$ direction). (a) and (d) First and second upper valence states; (b) and (e) third and fourth upper valence states; (c) and (f) fifth and sixth upper valence states for the unstrained and strained systems, respectively. The magenta and turquoise spheres show the iodine and chromium atoms, respectively.